

Effect of In doping on the evolution of microstructure, magnetic properties and corrosion resistance of NdFeB magnets

Yuhao Li(李豫豪), Xiaodong Fan(范晓东), Zhi Jia(贾智), Lu Fan(范璐), Guangfei Ding(丁广飞), Xincai Liu(刘新才), Shuai Guo(郭帅), Bo Zheng(郑波), Shuai Cao(曹帅), Renjie Chen(陈仁杰), and Aru Yan(闫阿儒)
Citation: Chin. Phys. B, 2024, 33 (**3**): 037508. DOI: 10.1088/1674-1056/ad0e5c
Journal homepage: http://cpb.iphy.ac.cn; http://iopscience.iop.org/cpb

What follows is a list of articles you may be interested in

Enhanced resonance frequency in Co_2FeAl thin film with different thicknesses grown on flexible graphene substrate

Cai Zhou(周偲), Shaokang Yuan(袁少康), Dengyu Zhu(朱登玉), Yuming Bai(白宇明), Tao Wang(王韬), Fufu Liu(刘福福), Lulu Pan(潘禄禄), Cunfang Feng(冯存芳), Bohan Zhang(张博涵), Daping He(何大平), and Shengxiang Wang(汪胜祥)
Chin. Phys. B, 2024, 33 (**3**): 037506. DOI: 10.1088/1674-1056/acfafa

Mechanical and magnetocaloric adjustable properties of Fe_3O_4/PET deformed nanoparticle film

Fengguo Fan(范凤国) and Lintong Duan(段林彤)
Chin. Phys. B, 2024, 33 (**3**): 037502. DOI: 10.1088/1674-1056/acf280

Effect of CeO_2 doping on the coercivity of 2:17 type SmCo magnets

Xiao-Lei Gao(高晓磊), Zhuang Liu(刘壮), Guang-Qing Wang(王广庆), Chao-Qun Zhu(竺超群), Wen-Xin Cheng(程文鑫), Ming-Xiao Zhang(张明晓), Xin-Cai Liu(刘新才), Ren-Jie Chen(陈仁杰), and A-Ru Yan(闫阿儒)
Chin. Phys. B, 2023, 32 (**9**): 097504. DOI: 10.1088/1674-1056/acaa24

Prediction of a monolayer spin-spiral semiconductor: CoO with a honeycomb lattice

Jie Zhang(张杰), Shunuo Song(宋姝诺), Yan-Fang Zhang(张艳芳),Yu-Yang Zhang(张余洋), Sokrates T. Pantelides, and Shixuan Du(杜世萱)
Chin. Phys. B, 2023, 32 (**8**): 087508. DOI: 10.1088/1674-1056/acd923

Fine-grained NdFeB magnets prepared by low temperature pre-sintering and subsequent hot pressing

Ju Jin-Yun (剧锦云), Tang Xu (唐旭), Chen Ren-Jie (陈仁杰), Wang Jin-Zhi (汪金芝), Yin Wen-Zong (尹文宗), Lee Don (李东), Yan A-Ru (闫阿儒)
Chin. Phys. B, 2015, 24 (**1**): 017504. DOI: 10.1088/1674-1056/24/1/017504

Effect of In doping on the evolution of microstructure, magnetic properties and corrosion resistance of NdFeB magnets

Yuhao Li(李豫豪)[1,2], Xiaodong Fan(范晓东)[2], Zhi Jia(贾智)[2,3], Lu Fan(范璐)[2], Guangfei Ding(丁广飞)[2,3], Xincai Liu(刘新才)[1,†], Shuai Guo(郭帅)[2,‡], Bo Zheng(郑波)[2,§], Shuai Cao(曹帅)[2], Renjie Chen(陈仁杰)[2,3], and Aru Yan(闫阿儒)[2,3]

[1] *School of Materials Science and Chemical Engineering, Ningbo University, Ningbo* 315211, *China*

[2] *CISRI & NIMTE Joint Innovation Center for Rare Earth Permanent Magnets, Ningbo Institute of Materials Technology and Engineering, Chinese Academy of Sciences, Ningbo* 315201, *China*

[3] *University of Chinese Academy of Sciences, Beijing* 100049, *China*

(Received 7 August 2023; revised manuscript received 20 November 2023; accepted manuscript online 21 November 2023)

The grain boundary phase affects the magnetic properties and corrosion resistance of sintered NdFeB magnets. In this work, a small amount of In was added to NdFeB magnets by induction melting to systematically investigate its effect on the evolution of the microstructure, magnetic properties and corrosion resistance of NdFeB magnets. Microstructural analysis illustrated that minor In addition generated more grain boundary phases and an abundant amorphous phase at the triple-junction grain boundary. While the addition of In failed to enhance the magnetic isolation effect between adjacent matrix grains, its incorporation fortuitously elevated the electrochemical potential of the In-containing magnets. Besides, during corrosion, an In-rich precipitate phase formed, hindering the ingress of the corrosive medium into the magnet. Consequently, this significantly bolstered the corrosion resistance of the sintered NdFeB magnets. The phase formation, magnetic properties and corrosion resistance of In-doped NdFeB magnets are detailed in this work, which provides new prospects for the preparation of high-performance sintered NdFeB magnets.

Keywords: In-doping, NdFeB magnets, magnetic properties, corrosion resistance

PACS: 75.50.Ww, 68.35.bd, 82.45.Bb, 75.60.Ej **DOI:** 10.1088/1674-1056/ad0e5c

1. Introduction

Since the inception of NdFeB permanent magnets in the 1980s, they have found extensive applications across diverse fields.[1–5] With expanding demand, the need for information on the magnetic properties and corrosion resistance of NdFeB continues.[5–9] Studies have shown that optimizing the microstructure of magnets is a common approach to improving magnetic properties.[10–14] Corrosion resistance during practical application is another important indicator for evaluating NdFeB magnets.[15,16] Conventional corrosion processes preferentially dissolve several low-potential grain boundary phases such as Nd-rich and B-rich ones.[17,18] To prevent corrosion, it is necessary to mitigate the potential difference between the grain boundary phase and the matrix phase to improve the corrosion resistance of a magnet.[19,20] Therefore, exploring how to efficiently improve the magnetic properties and corrosion resistance of NdFeB magnets is an important research topic.

It has been demonstrated that the addition of non-magnetic alloy additives, such as Nd-rich and Pr-rich alloys, can optimize the microstructure to enhance magnetic properties and corrosion resistance.[10–14,21,22] Furthermore, enhancing both magnetic properties and corrosion resistance is a challenge, and one of the properties may deteriorate.[18,20,23] Currently, the addition of microelements during the melting process has been widely used to optimize magnetic properties.[10,24] For example, Al and Ga have been added, resulting in the formation of continuous and thick grain boundaries, thereby increasing the coercivity via the demagnetization coupling strengthening mechanism. The addition of alloying additives containing Al and Ga also enhanced the corrosion resistance of NdFeB magnets.[25–27] This method diminishes the disparity in electrochemical potential between the ferromagnetic phase and the intergranular matrix phase, subsequently attenuating the impetus for electrochemical corrosion.[28–30]

The element In is the same main group as Al and Ga and has similar chemical properties. Therefore, we speculate that In doping of NdFeB magnets will produce similar effects to the addition of Al and Ga, but this has rarely been studied systematically. In this work, a small amount of In was introduced to sintered NdFeB magnets during induction melting to examine its impact on microstructure, magnetic properties and corrosion resistance. It is expected that In and Ga will have similar effects in NdFeB, with amorphous thin-walled grain boundary phases appearing at grain boundaries that may en-

†Corresponding author. E-mail: liuxincai@nbu.edu.cn
‡Corresponding author. E-mail: gshuai@nimte.ac.cn
§Corresponding author. E-mail: zhengbo@nimte.ac.cn

© 2024 Chinese Physical Society and IOP Publishing Ltd

hance the magnetic properties and corrosion resistance of the magnet. Microstructural analysis was utilized in this work to clarify the mechanism of the effect of In doping on the magnetic properties and corrosion resistance of sintered NdFeB magnets.

2. Experimental details

The raw materials were industrially pure (99.9%) Fe, Fe–B, Nd, Co, Al, Cu and Zr. Alloys with nominal compositions of $Nd_{30.5}(Fe,Co)_{68.6}M_{0.5}B_{0.94}$ and $Nd_{30.5}(Fe,Co)_{67.56}In_{0.5}M_{0.5}B_{0.94}$ (wt%, where M = Al, Cu or Zr) were denoted as 0In and 0.5In samples, respectively. Alloys were melted by induction melting under a protective atmosphere of high-purity Ar gas and then cast onto rotating copper rollers. The obtained 0In and 0.5In alloys were in the form of strip-cast (SC) flakes. The SC flakes were then crushed into coarse powders using hydrogen decrepitation, and these were further refined by jet milling under a nitrogen atmosphere. The magnetic particles were then crushed by hydrogen decrepitation and jet milling to give an average particle size of 2.5–2.8 μm. The magnetic particles of two different compositions were then compacted in a 1.8 T magnetic field then isostatically compacted at a pressure of 160–170 MPa. Afterwards, the green compacts were sintered at 1080–1090 °C for 4 h in a vacuum with gas quenching, followed by post-annealing for 2 h at 900 °C and 500–550 °C, respectively. Finally, magnets of 7 mm diameter and 5 mm thickness were prepared by cutting.

The room-temperature demagnetization curves of the magnets were measured using a pulsed-field magnetometer (HIRST PFM14.CN). Observation of the microstructure of the samples was carried out in the backscattering mode of a scanning electron microscope (SEM; FEI Quanta FEG 250), and energy dispersive spectroscopy (EDS) was used to quantitatively analyze the elemental distribution. Using a Talos F200X scanning/transmission electron microscope the detailed microstructure and elemental distribution of the localized phases was further investigated by scanning/transmission electron microscopy and energy dispersive x-ray spectroscopy. Electrochemical polarimetry (Modulab XM potentiostat) was performed at 25°, and all experiments were conducted in a standard three-electrode cell consisting of a working electrode of NdFeB, a saturated silver chloride reference and a Pt counter electrode. The experiments were performed in an aerated 3.5 mass% NaCl solution. After the opening point position (open circuit potential) reached a stable state (usually after soaking in an electrolytic cell for 30 min), the polarization curve was recorded at a scanning rate of 0.5 $mV{\cdot}s^{-1}$ (the test time was 2 h), from negative potential to positive potential. All electrochemical tests were repeated twice under the same conditions to ensure reasonable reproducibility. Before the experiment, each sample was cleaned and its initial weight was recorded. The samples were placed in a weight loss instrument (HAST EHS-221M) with saturated humidity and a temperature of 130 ° for 72 h for high-pressure cooking testing. After the test, the surface of each sample was cleaned and the weight loss of each sample was recorded.

3. Results and discussion

3.1. Microstructure evolution during strip-casting, sintering and annealing processes

Figure 1 shows the backscattered electron (BSE) SEM images of the SC alloys. Both 0In and 0.5In alloys are composed of layered matrix phases (gray stripes) and rare-earth-rich (RE-rich) phases (white stripes), consistent with previously reported phenomena.[31–33] The corresponding Fe and Nd elemental mapping distributions are clearly visible, with Fe distributed as strips in the matrix phase and Nd enriched at grain boundaries. It is important to note that the morphology of the RE-rich phase of the 0.5In magnet is distinct from that of the 0In magnet. First, the width and length of the columnar crystals in the matrix phase of the In-doped magnet are narrower and shorter. Second, the grain boundary phase is discontinuous and inhomogeneous. The grain boundary phase of 0.5In SC is shorter than that of 0In SC alloy, and the terminals are concentrated into distinct spheres (regions 1 and 2 in Fig. 1(d)). Third, In is enriched in the grain boundary phase and remains concentrated in spheres in the grain boundary phase. The distribution of In in the grain boundary phase is extremely discontinuous and inhomogeneous. The segregation distribution of In is directly responsible for the discontinuity and inhomogeneity of the grain boundary phase of the 0.5In magnet. This phenomenon may extend to affect the subsequent sintering and annealing processes and may impact the magnetic properties of the magnet. The microstructural differences of SC alloy (0.5In) are related to various factors. Firstly, because the added amount of In only accounts for 0.5 wt% of the overall content it only enters some Nd-rich grain boundary phases. The microstructure of the strip-cast alloy is related to the melting temperature and cooling rate, and under these conditions the distribution of In at grain boundaries tends to converge in some Nd-rich phases, with little effect on the matrix phase.

Figure 2 shows the BSE SEM and EDS images at different magnifications in 0In (Figs. 2(a) and 2(b)) and 0.5In (Figs. 2(c) and 2(d)) sintered magnets. For the 0In and 0.5In sintered magnets, Fe atoms are distributed in the matrix phase and Nd atoms are enriched at grain boundaries, consistent with the elemental distribution in SC alloys. Additionally, In atoms segregate in the triple-junction phase, Moreover, under low magnification (Figs. 2(a) and 2(c)), there are more grain

boundaries in the 0.5In sintered magnet than in the 0In one. However, the grain boundaries of the 0.5In magnet are still not continuous and the matrix grains are not effectively separated from each other. The reason for this phenomenon is that In accumulates and forms defects at the grain boundary. In fact, defects cannot be eliminated by sintering the magnet.

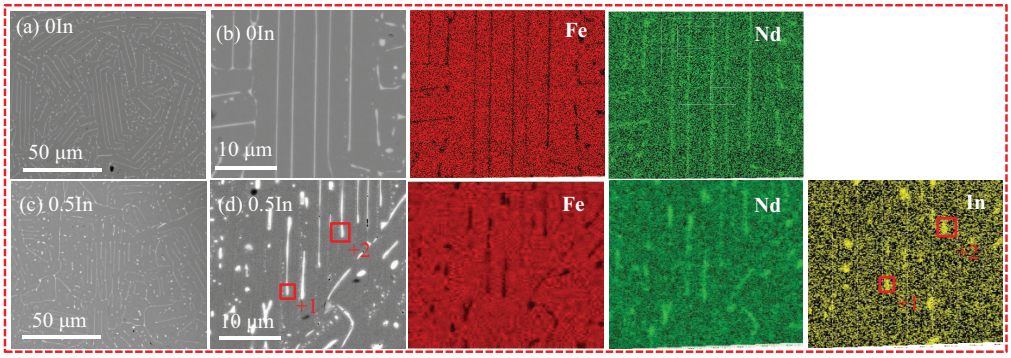


Fig. 1. BSE SEM images showing elemental mapping of Fe, Nd and In for (a), (b) strip-cast 0In NdFeB and (c), (d) strip-cast 0.5In doped NdFeB.

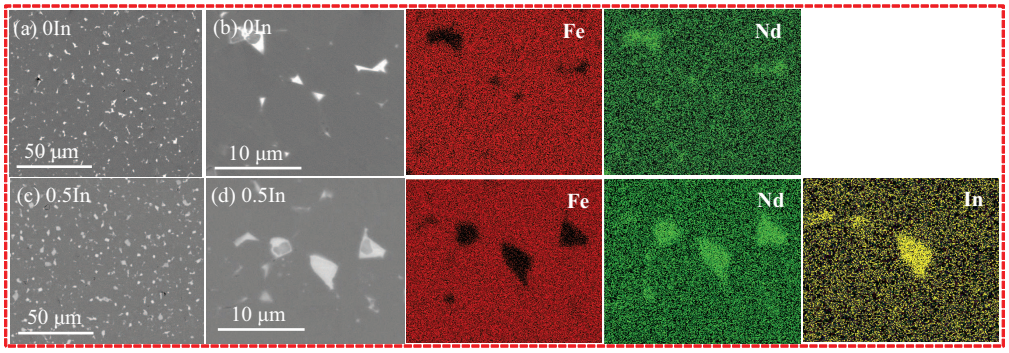


Fig. 2. BSE SEM images of (a), (b) 0In NdFeB sintered magnet and (c), (d) 0.5In NdFeB sintered magnet and the corresponding EDS elemental mapping of Fe, Nd and In.

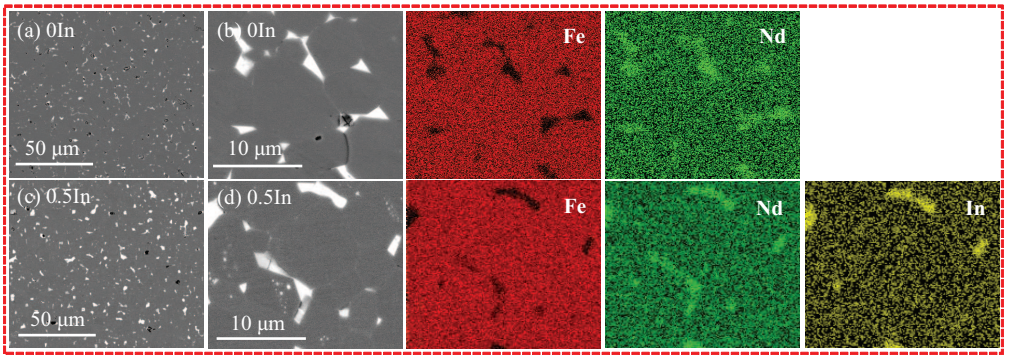


Fig. 3. Different magnifications of BSE SEM images of (a), (b) 0In NdFeB annealed magnet and (c), (d) 0.5In NdFeB annealed magnet and the corresponding EDS elemental mapping of Fe, Nd and In.

The structural characteristics and elemental distribution of 0In and 0.5In annealed magnets are shown in Fig. 3. The distributions of Fe, Nd and In in the annealed magnets are similar to those in the sintered magnets. However, the annealed 0.5In magnet still has more grain boundary phases than the annealed 0In magnet (Figs. 3(a) and 3(c)). The increase in the grain boundary phase is due to melting of the defect region at the grain edge of the matrix phase upon magnet annealing, and also to the introduction of non-magnetic elements. Observations at high magnification reveal that the 0In magnet exhibits a continuous grain boundary phase, effectively isolating the adjacent matrix phases. However, the 0.5In magnet does not form a considerable number of continuous grain boundary phases to support the magnetic isolation effect, although it has more grain boundary phases. In addition, it is not difficult to see that a large number of blocky In agglomerates are eliminated at the grain boundaries. Segregation of In at grain boundaries in sintered and annealed magnets also occurs for various reasons. On the one hand, during the strip-casting stage it is observed that some Nd-rich phases contain In while others have no In. During subsequent hydrogen decrepitation and jet milling, the alloy flakes are crushed without affecting

the phase structure. Therefore, this segregation phenomenon continues until the sintering and annealing stages. On the other hand, the fluidity of In in NdFeB is poor,[34] and the sintering and annealing temperatures cannot change the distribution of In-rich phases stacked at the triple-junction grain boundaries. Therefore, the segregation of In runs through the entire process of magnet preparation.

3.2. TEM microstructural characterization

Transmission electron microscopy (TEM) was utilized to clarify the composition distribution of the triple-junction phase in more detail. Figure 4 depicts the detailed microstructural characteristics of annealed 0In and 0.5In magnets. The high-angle annular dark-field scanning TEM image of the annealed 0In sample reveals three matrix phase grains surrounding the triple-junction phase (Fig. 4(a)). The corresponding elemental distributions of Fe and Nd reveal that Fe is enriched in the grains of the matrix phase while Nd is enriched in the triple-junction phase, as shown in Figs. 4(d) and 4(e). A high-resolution TEM (HRTEM) image of the A1 area (red circle) of the grain boundary phase GB1 is shown in Fig. 4(b), and the grain boundary phase hcp-RE_2O_3 structure in the selected area (electron) diffraction (SAED) pattern is shown in Fig. 4(c).

Bright-field TEM images of the 0.5In annealed magnet are shown in Fig. 4(f). The grain boundary phase GB2 of the 0.5In annealed magnet has Fe-poor and Nd-rich regions, as shown in Figs. 4(i) and 4(j), respectively. Figure 4(k) shows that In is also enriched in the GB2 grain boundary region, consistent with the BSE SEM observations (Fig. 3). In addition, the A2 area (yellow circle) shows the grain boundary structure of GB2, which is significantly different from that of GB1. Figure 4(h) shows an HRTEM image of the A2 area, which presents a ring-shaped diffraction pattern. Accordingly, the grain boundary area of the 0.5In sample remains amorphous. Following TEM characterization, in-depth analysis was conducted on the phase structure and distribution of 0In and 0.5In samples. The distribution of In in sintered magnets is similar to that of Ga, and both form amorphous phases. However, combined with BSE EDS analysis, it can be determined that In does not form thick and uniform thin-walled grain boundary phases in the grain boundaries, but rather accumulates in triple-junction grain boundaries that cannot provide effective magnetic isolation. The coercivity of NdFeB is a sensitive parameter of the structure, and considering the characteristics of In distribution it may be less helpful for determining the magnetic properties.

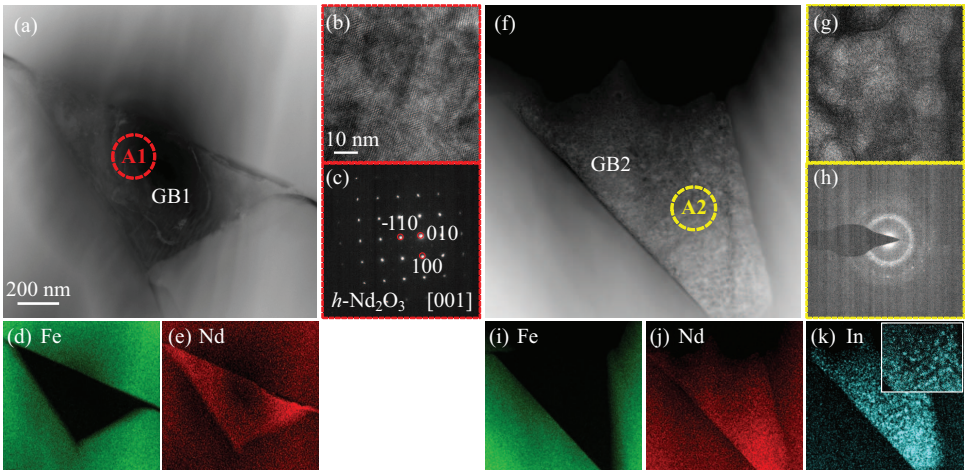


Fig. 4. (a) High-angle annular dark-field (HADDF) STEM image of a 0In annealed magnet and (d), (e) EDS elemental maps of the triple junction. (b) HRTEM image of region A1 in (a) and (c) SAED pattern of region A1 in (b). (f) HADDF STEM image of a 0.5In annealed magnet and (i)–(k) EDS elemental maps of the triple junction. (g) HRTEM image of region A2 in (f) and (h) SAED pattern of region A2 in (f).

3.3. Magnetic properties

The microstructure of magnets has a significant influence on their magnetic properties; therefore we studied the magnetic properties of NdFeB magnets in detail. Figure 5(a) shows the room-temperature demagnetization curves of 0In and 0.5In magnets at annealed at different temperatures, and their magnetic properties are summarized in Table 1. Figure 5(b) compares the magnetic properties of the 0In and 0.5In annealed magnets at room temperature. The coercivity (H_{cj}) of the 0.5In magnet is 11.24 kOe, which is slightly lower (by 0.32 kOe) than that of the 0In magnet (11.56 kOe), and the maximum magnetic energy product $(BH)_{max}$ is 47.48 MGOe and 47.08 MGOe, respectively In fact, H_{cj} of NdFeB is highly sensitive to microstructure, such as the grain size, intergranular phase composition and structure. The addition of a small amount of In causes significant changes in the microstructure of the magnet. Moreover, the amorphous structure is segregated in the Nd-rich phase, which prevents effective magnetic isolation. The addition of non-magnetic In led to a small reduction in the remanence (B_r) and $(BH)_{max}$, similar to the phenomena reported previously upon the addition of Al and Ga elements.[31,32]

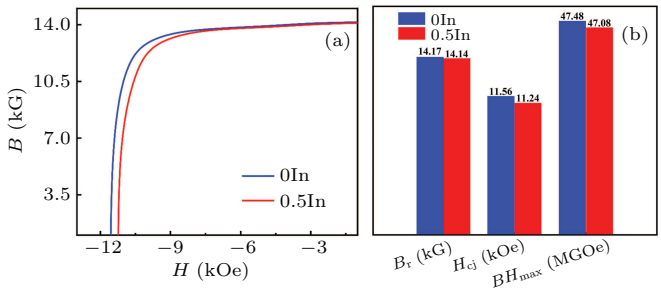


Fig. 5. (a) Room-temperature demagnetization curves of optimized annealed 0In and 0.5In magnets. (b) B_r, H_{cj}, and $(BH)_{max}$ of 0In and 0.5In magnets.

Table 1. Magnetic properties derived from the demagnetization curves for the annealed 0In and 0.5In magnets.

Sample	B_r (kG)	H_{cj} (kOe)	$(BH)_{max}$ (MGOe)
Annealed 0In	14.17	11.56	47.48
Annealed 0.5In	14.14	11.24	47.08

3.4. Corrosion resistance

The corrosion resistance of NdFeB magnets is closely related to their microstructure and phase composition, particularly the composition and structure of the intergranular phase.[35,36] Figure 6(a) shows the potentiodynamic polarization curves of 0In and 0.5In magnets before and after treatment with 3.5 mass% NaCl solution; the corresponding fitting results are summarized in Table 2. The BSE SEM and corresponding elemental distributions of 0In and 0.5In magnets after the soaking treatment are shown in Figs. 6(b)–6(d). The surface of the 0In magnet has more pits and inhomogeneous pores (Figs. 6(b) and 6(c)), while the 0.5In magnet has better surface characteristics than the 0In magnet (Figs. 6(c) and 6(d)). The original corrosion potential of the 0In magnet was −0.77 V. After In doping, the corrosion potential of the 0.5In magnet changed to −0.76 V. The corrosion current density of the 0In magnet was 4.35×10^{-4} A·cm^{-2}, and after In doping the current density dropped sharply to 1.54×10^{-4} A·cm^{-2}. After soaking 0In and 0.5In magnets in 3.5 mass% NaCl solution for 48 h, the corrosion potential of the 0In magnet changed to −0.82 V, but the corrosion potential of the 0.5In magnet remained at −0.78 V. Furthermore, the corrosion current density dropped from 7.72×10^{-4} A·cm^{-2} for the 0In magnet to 3.68×10^{-4} A·cm^{-2} for the 0.5In magnet.

Figures 6(b) and 6(c) illustrate the inhomogeneous pits on the magnet surface after the 0In sample was soaked in 3.5 mass% NaCl solution. Elemental distribution also confirms that these pits are due to the absence of grain boundary phases, and an increased porosity between the grains of the matrix phase is observed, making separation from the bulk more likely. In contrast, after soaking, the surface of the 0.5In magnet also has pits but is flatter than the 0In sample; the elemental distributions also indicate that the matrix phase grains are agglomerated with each other. Moreover, In is widely distributed on the surface of the matrix phase grains, so it can be assumed that the enhancement of the corrosion resistance of the 0.5In sample is due to the improved doping with In.

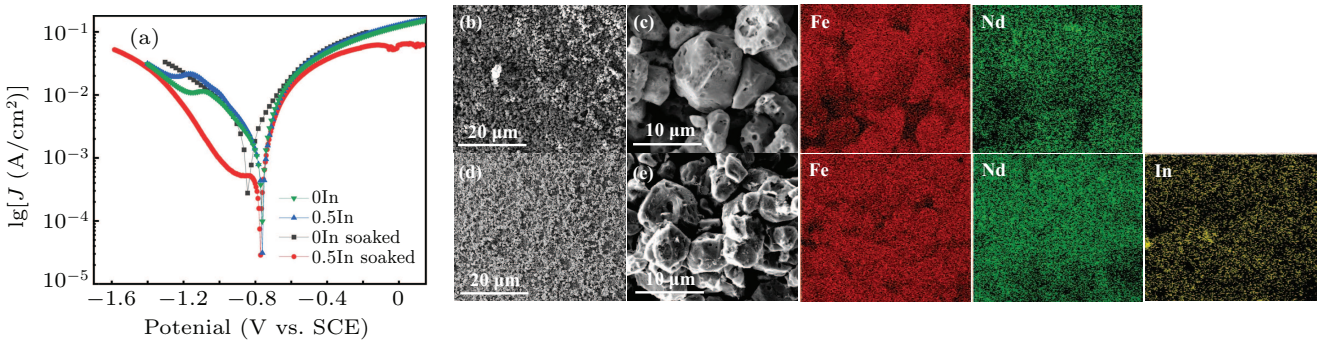


Fig. 6. (a) Potentiodynamic polarization curves for 0In and 0.5In magnets without and with 48 h soaking in 3.5 mass% NaCl solution. Different magnifications of BSE SEM images of (b), (c) 0In and (d), (e) 0.5In annealed magnets after 48 h soaking and the corresponding EDS elemental mappings of Fe, Nd and In.

Table 2. Results for 0In and 0.5In magnet potentiodynamic polarization curves without and with 48 h soaking in 3.5 mass% NaCl solution.

Sample	E_{corr} (V)	I_{corr} (A·cm^{-2})
0In	−0.77	4.35×10^{-4}
0.5In	−0.76	1.54×10^{-4}
0In soaked	−0.82	7.72×10^{-4}
0.5In soaked	−0.78	3.68×10^{-4}

To verify the effect of In doping on the corrosion resistance of the magnets, further weight reduction experiments were performed. Figures 7(a)–7(d) show the surface morphology and corresponding Fe, Nd, O and In distributions in 0In and 0.5In samples after weight loss. Figure 7(e) shows the energy spectrum of 0.5In samples after weight loss, Fig. 7(f) shows the mass and mass difference of the two samples before and after weight loss and Fig. 7(g) shows powder XRD spectra of the two samples after weight loss. In Figs. 7(a)–7(d) the 0In samples show severe corrosion on the surface and serious grain damage. On the other hand, the surface of the 0.5In sample is very flat, and a large number of bright particles can be observed under high magnification; the elemental distribution and energy spectrum results indicate that the bright particles are In-rich precipitates. Figure 7(f) shows that after weight loss, the mass loss of the 0In sample was 1.819 mg·cm^{-3},

while that of the 0.5In sample was only 0.930 mg·cm^{-3}. This fully demonstrates that In doping has a significant effect on the corrosion resistance of the magnet. Figure 7(g) shows the XRD results of the two samples after corrosion, and reveals that several In-rich diffraction peaks appear in the 0.5In sample, consistent with the BSE EDS results.

Combining electrochemical and weight loss experiments, it can be confirmed that the corrosion resistance of magnets containing In is significantly enhanced. This is attributed to the fact that In doping improves the electrochemical potential of the magnet and reduces the potential difference between the grains of the matrix phase and the grain boundary phase. This is most likely due to the substitution of some metals in the magnet by In, which increases the total potential. The results of weight loss experiments also show that the corrosion resistance of In is significantly improved. During corrosion of a NdFeB magnet, the Nd- and B-rich phases are corroded preferentially, and the In-rich grain boundary phase precipitates into the In-rich oxide, preventing the corrosive medium from entering the inside of the magnet, blocking the corrosion channel, slowing down the corrosion rate and significantly improving the corrosion resistance of the magnet.

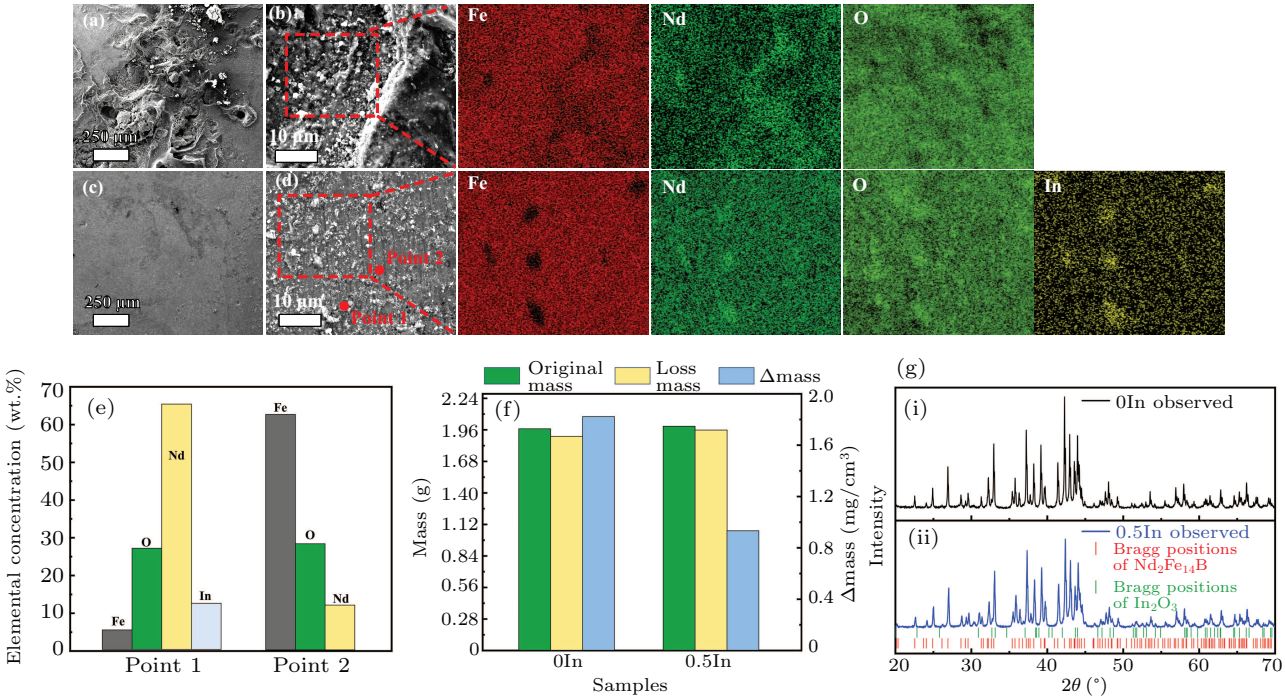


Fig. 7. (a)–(d) Surface morphology and corresponding Fe, Nd, O and In distributions of the 0In and 0.5In samples after weight loss. (e) Energy spectrum of the 0.5In sample. (f) Mass and mass difference of the two samples before and after weight loss. (g) XRD patterns of the two samples after weight loss.

4. Conclusion and perspectives

The magnetic properties, corrosion resistance and microstructural characteristics of sintered NdFeB magnets without and with 0.5 wt% In doping were investigated. This work fills the knowledge gap regarding the microstructural evolution of In-doped NdFeB magnets through detailed and systematic observations and characterizations. Additionally, the effect of In doping on the corrosion resistance of sintered NdFeB magnets was analyzed.

From observations of the microstructure, it was seen that the 0In and 0.5In magnets have similar phase structures. However, due to the inherent properties and distribution characteristics of In, subsequent heat treatment could not eliminate In segregation. Although In doping increases the proportion of grain boundary phases, most of the grain boundary phases do not form continuous and uniform thin-walled grain boundaries but instead form aggregates at the triple-junction boundary, which is not conducive to magnetic enhancement. In addition, In doping increases the electrochemical potential at the magnet and leads to the formation of In-rich oxide precipitates during corrosion, blocking the corrosion channels and significantly improving corrosion resistance. Therefore, follow-up work should focus on the relationship between the addition of In and magnetic properties, optimize the processing conditions for the preparation of strip-cast alloy flakes, optimize the structure and prepare sintered magnets with excellent magnetic properties and strong corrosion resistance.

Acknowledgements

This work was funded by Ningbo Key R&D Plan and "Unveiling and Leading" (Grant No. 2023Z093), Ningbo Science and Technology Innovation 2025 Major Special Project (Grant No. 2022Z106), and Hezhou City Central Leading Local Science and Technology Development Special Fund Project (Grant No. HK ZY2022002).

References

[1] Prosperi D, Bevan A I, Ugalde G, Tudor C O, Furlan G, Dove S, Lucia P and Zakotnik M 2018 *J. Magn. Magn. Mater.* **460** 448

[2] Ma B M, Herchenroeder J W, Smith B, Suda M, Brown D N and Chen Z 2002 *J. Magn. Magn. Mater.* **239** 418

[3] Zhang Y X, Zhao Y, Hu W, Wang X F and Yang R S 2023 *J. Alloys Compd.* **934** 167862

[4] Ya C S, M G Zhu, W Liu, R Han, W C Zhang, Y F Li and W Li 2017 *Chin. Phys. B* **26** 107501

[5] Liu W F, Zhang M G, Zhang K Q, Zhang H J, Xu X H and Chai Y S 2016 *Chin. Phys. B* **25** 117506

[6] Xie Y H, Cao S, Cao X J, Wu T F, Kou M P, Jia Z, Ding G F, Guo S, Chen R J, Liu X C, Yan A R and Xu Z Y 2023 *J. Alloys Compd.* **931** 167562

[7] Li L, Tirado A, Conner B S, Chi M F, Elliott A M, Rios O, Zhou H D and Paranthaman M P 2017 *J. Magn. Magn. Mater.* **438** 163

[8] Fan S N, Wang Z X, Jin Z H, Ding G F, Fan X D, Cao S, Guo S, Zheng B, Chen R J, Yan A R and Meng B 2022 *J. Alloys Compd.* **896** 163127

[9] Ze T Shu, B Z, G F Ding, S Cao. Liao J H Di, S Guo, R J Chen, A R Yan and L S 2020 *Chin. Phys. B* **29** 57501

[10] Ding J J, Xu B J and Ling G P 2014 *Appl. Surf. Sci.* **305** 309

[11] Derewnicka-Krawczynska D, Ferrari S, Bilovol V, Pagnola M, Morawiec K and Saccone F D 2018 *J. Magn. Magn. Mater.* **462** 83

[12] Okamoto S, Miyazawa K, Yomogita T, Kikuchi N, Kitakami O, Toyoki K, Billington D, Kotani Y, Nakamura T, Sasaki T, Ohkubo T, Hono K, Takada Y, Sato T, Kaneko and Y Kato 2019 *Acta Mater.* **178** 90

[13] Woodcock T G, Ramasse Q M, Hrkac G, Shoji T, Yano M, Kato A and Gutileisch O 2014 *Acta Mater.* **77** 111

[14] Sepehri-Amin H, Li W F, Ohkubo T, Nishiuchi T, Hirosawa S and Hono K 2010 *Acta Mater.* **58** 1309

[15] Feng Q, Huang Y, Li H, Yu J Y, Wang C Y, Wu Z, Yao Y, Hou Y, Li W, Ma L and Yu H 2023 *J. Alloys Compd.* **940** 168827

[16] Peng B X, Jin J Y, Liu Y S, Lu C X, Li L W and Yan M 2020 *Corros. Sci.* **177** 108972

[17] Zhang P, Ma T, Liang L and Yan M 2014 *Mater. Chem. Phys.* **147** 982

[18] Zhang K, Fan E, He J, Li X and Huang Y 2021 *J. Magn. Magn. Mater.* **538** 168309

[19] Dai J L, Yang Z X and Liu Q 2020 *Materials* **13** 4360

[20] Li B, Zhou X S, Chen X P, Fu S, Wang X D and Zhao D L 2022 *Materials* **15** 7523

[21] Billington D, Okazaki H, Toyoki K, Kotani Y, Takada Y, Sato T, Kaneko Y, Kato A, Sasaki T T, Ohkubo T, Hono K and Nakamura T 2021 *Acta Mater.* **205** 116517

[22] Li J, Tang X, Sepehri-Amin H, Sasaki T T, Ohkubo T and Hono K 2020 *Acta Mater.* **187** 66

[23] Tao J, Liu, B, Zhang P, Xu G, Lv J, Huang J, Yan J, Sun W, Li B, Wang D and Wu Y 2023 *J. Rare Earths* **41** 1203

[24] Zhang K, Fan E, He J, Li X and Huang Y 2021 *J. Magn. Magn. Mater.* **538** 168309

[25] Ni J J, Zhang Z Y, Liu Y, Jia Z F, Huang B X and Yin Y B 2016 *Physica B* **499** 64

[26] El-Moneim A A, Gebert A, Uhlemann M, Gutfleisch O and Schultz L 2002 *Corros. Sci.* **44** 1857

[27] Huang Y, Li H, Zuo M, Tao L, Wang W, Zhang J, Tang Q and Bai P 2016 *J. Magn. Magn. Mater.* **409** 39

[28] Ku N C, Qin C D, Yu C C and Ng D H L 1996 *IEEE Trans. Magn.* **32** 4407

[29] Assis O B G, Sinka V, Ferrante M and Oliveira I L 1995 *J. Alloys Compd.* **218** 263

[30] Liu W Q, Yue M, Zhang D T, Zhang J X and Liu X B 2009 *J. Appl. Phys.* **105** 07A709

[31] Guo S, Zhou Q Y, Chen R J, Lee D and Yan A R 2011 *J. Appl. Phys.* **109** 07A734

[32] Guo S, Liu Y H, Chen B C, Yan C J, Chen R J, Lee D and Yan A R 2012 *J. Appl. Phys.* **111** 07A740

[33] Fan X D, Ding G F, Chen K, Guo S, You C Y, Chen R J, Lee D and Yan A R 2018 *Acta Mater.* **154** 343

[34] Noguchi D, Takeda O, Zhu H and Sugimoto S 2021 *J. Magn. Magn. Mater.* **539** 168407

[35] Mottram R S, Williams A J and Harris I R 2000 *J. Magn. Magn. Mater.* **217** 27

[36] Rada M, Gebert A, Mazilu I, Khlopkov K, Gutfleisch O, Schultz L and Rodewald W 2006 *J. Alloys Compd.* **415** 111